DNA Multiphoton Absorption Generates Localized Damage for Studying Repair Dynamics in Live Cells

Matthew K. Daddysman[†] and Christopher J. Fecko[†*]
[†]Department of Chemistry, University of North Carolina at Chapel Hill, Chapel Hill, North Carolina

ABSTRACT Investigations into the spatiotemporal dynamics of DNA repair using live-cell imaging are aided by the ability to generate well defined regions of ultravioletlike photolesions in an optical microscope. We demonstrate that multiphoton excitation of DNA in live cells with visible femtosecond pulses produces thymine cyclopyrimidine dimers (CPDs), the primary ultraviolet DNA photoproduct. The CPDs are produced with a cubic to supercubic power dependence using pulses in the wavelength range from at least 400 to 525 nm. We show that the CPDs are confined in all three spatial dimensions, making multiphoton excitation of DNA with visible light an ideal technique for generating localized DNA photolesions in a wide variety of samples, from cultured cells to thicker tissues. We demonstrate the utility of this method by applying it to investigate the spatiotemporal recruitment of GFP-tagged topoisomerase I (TopI) to sites of localized DNA damage in polytene chromosomes within live cells of optically thick *Drosophila* salivary glands.

INTRODUCTION

The study of DNA damage repair has long been aided by experiments that examine cellular responses to DNA lesions produced by ultraviolet (UV) light. All of the nucleic acids absorb 200–300 nm light efficiently, but the main photoproducts that result from absorption of light in this spectral region are thymine cyclopyrimidine dimers (CPDs) (1,2). It is straightforward to create CPDs by exposing cells to the ~254-nm light emitted by low-pressure mercury vapor lamps, but this method results in a random spatial distribution of lesions. To investigate with fluorescence-based microscopy the spatiotemporal dynamics of proteins involved in the repair of CPDs in live cells, it is more desirable to create photolesions in spatially restricted, user-defined regions of cell nuclei.

Several methods to generate localized DNA damage have been investigated (3). Perhaps the most obvious option, irradiation by a focused UV laser (4), is somewhat limited by the relatively low numerical aperture of objective lenses that transmit UVC light. Furthermore, chromatic aberrations of these objectives, as well as the poor UV transmission of other common optical elements, prevent the easy pairing of UV sources with a conventional microscopy apparatus. More recently, localized DNA damage has been introduced by passing UVC light through 3- to 5-μm pores in a polycarbonate filter placed near the sample (5–8). However, when this method is applied to cultured mammalian cells, the spatial extent of DNA damage is still a considerable fraction of the nuclei. In addition, to investigate repair-protein recruitment to specific locations, it would be advantageous to be able to preselect the nuclear region to be damaged, which is difficult to do using the filter method. Finally, laser-based irradiation of presensitized cells in the 337–405 nm range efficiently generates damage, but the focus of this method is to form strand breaks preferentially over nitrogen-base photoproducts (9–12), which excludes the investigation of processes that repair UV lesions, such as nucleotide excision repair. This method also suffers from the potentially serious drawback that the sensitizing agent could perturb the natural response of the biological system. Ultimately, it is possible to localize the extent of DNA damage in only two dimensions using these methods; they do not offer confinement in the third (axial) dimension. The lack of axial confinement is acceptable for a thin monolayer of cultured cells; however, to selectively damage thick tissues or nuclei, a method providing axial confinement is necessary. As an alternative, multiphoton excitation of DNA has the potential to create spatially localized CPDs without the aforementioned limitations.

Nonresonant multiphoton absorption is the process by which a molecule exposed to a high photon flux interacts with two or more photons simultaneously, producing an excited state equivalent in energy to the summation of the energy of the interacting photons (13). Multiphoton microscopy takes advantage of this phenomenon by combining the nonlinear intensity dependence with a steeply decreasing intensity profile outside of the focal point of the objective lens to enhance imaging depth discrimination (14,15). Our group has previously demonstrated that DNA exhibits multiphoton absorption when exposed to visible femtosecond pulses in vitro (16); in contrast to its application for imaging purposes, multiphoton absorption of DNA photochemically produces lesions that are subject to cellular repair mechanisms (Fig. 1 *A*). Herein, we investigate the use of multiphoton absorption of visible light as a means to produce three-dimensionally localized thymine CPDs in cells, and we demonstrate its utility in studying the spatiotemporal recruitment of topoisomerase I (TopI) to sites of DNA

Submitted June 13, 2011, and accepted for publication September 23, 2011.
*Correspondence: cfecko@unc.edu
Editor: David P. Millar.

0006-3495/11/11/2294/10 $2.00
doi: 10.1016/j.bpj.2011.09.031

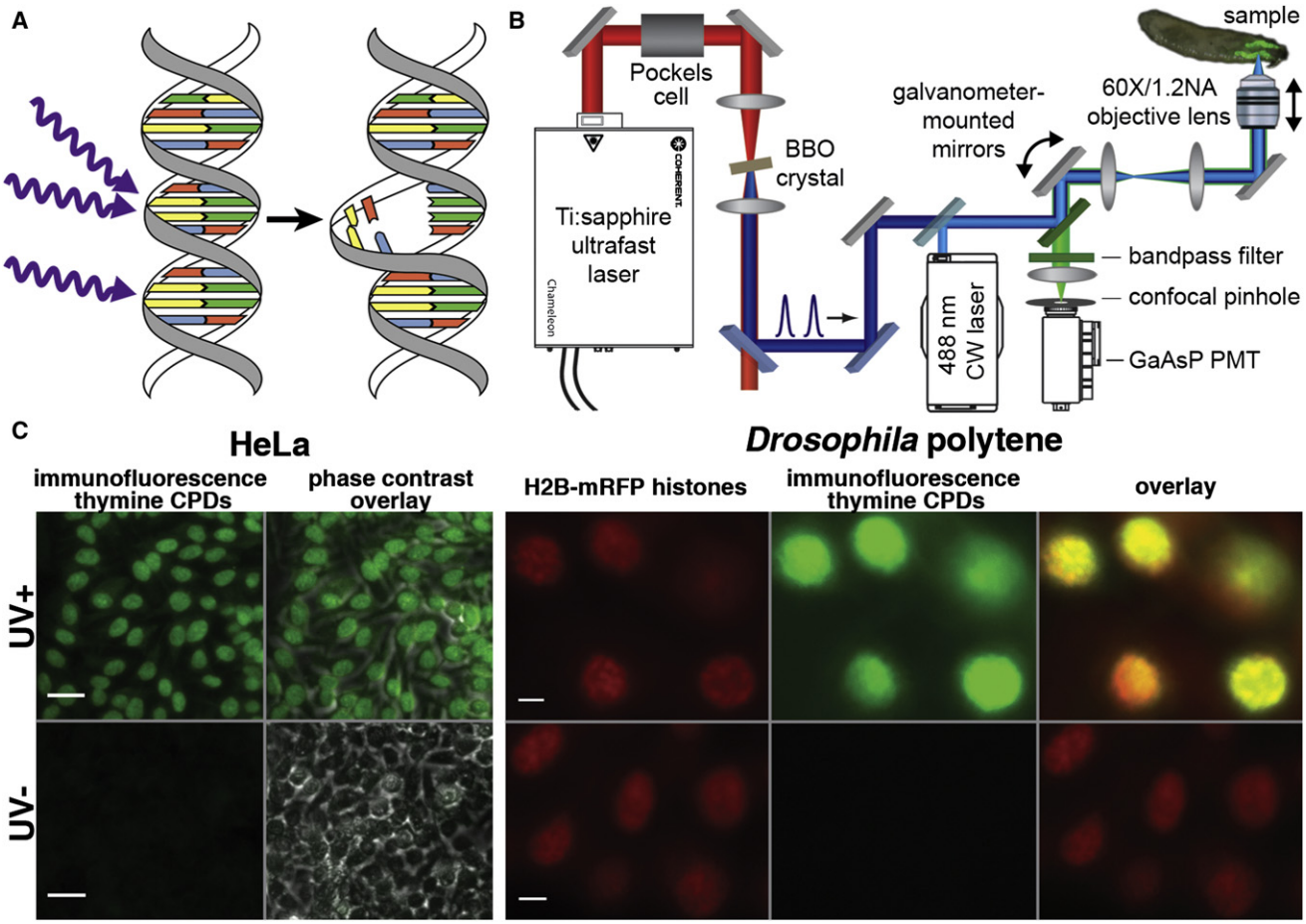

FIGURE 1 (*A*) Simultaneous absorption of two blue photons by DNA leads to the production of a thymine CPD. Interaction with a single blue photon does not affect the DNA. (*B*) Schematic of the apparatus used to irradiate and image cells. The near-IR output of a femtosecond Ti:sapphire laser is attenuated by a Pockels cell/polarizer and then frequency-doubled by a BBO crystal. Dichroic mirrors remove the fundamental before the beam, focused by a 60× 1.2 NA water-immersion objective lens, is scanned through the sample. A 488-nm CW laser can be introduced into the setup to perform control experiments. (*C*) Verification of thymine CPD detection using an immunochemical assay. Samples were irradiated with 1.6 kJ/m^2 (UV+, HeLa), 6.6 kJ/m^2 (UV+, *Drosophila*), or no (UV−) 254-nm UV radiation. After staining for thymine CPDs, the UV+ cells showed immunofluorescence that was at least an order of magnitude brighter than that of the control group and showed nuclear localization. In addition, the *Drosophila* fluorescence shows chromosomal localization, as indicated in the overlay with the H2B-mRFP image. Scale bars, 40 μm for HeLa and 20 μm for *Drosophila*.

damage. We refer to this method as damage induced by multiphoton excitation of DNA with visible light (DIMED-Vis).

We first establish that multiphoton absorption of visible light produces thymine-thymine CPDs in HeLa cells and in the polytene chromosomes of *Drosophila melanogaster* larval salivary gland cells. Our experiments focus ultrafast 400- to 525-nm pulses generated by frequency-doubling the output of a Ti:sapphire laser into cellular samples using a home-built multiphoton microscope (Fig. 1 *B*). The blue-green light itself is harmless to cells, but multiphoton absorption at the objective-lens focal point produces DNA photolesions. We use HeLa cells to characterize the wavelength and power dependence of our in vivo procedure and polytene chromosomes to demonstrate the localized nature of the lesions. Previous studies have found that ultrashort near-infrared (near-IR) pulses can also generate DNA damage in vivo (17,18) via multiphoton absorption; however, the irradiation conditions required to generate DNA damage with near-IR pulses also introduce other types of cellular damage, including apoptosis in some cases (19–22), or they require long pixel dwell times, which can be difficult to implement on conventional confocal laser scanning microscopes. Therefore, the use of ultrashort visible pulses, a method relatively harmless to cells, provides an alternative to near-IR wavelengths for generating three-dimensionally localized CPDs in cells with microsecond scan times and powers commonly used for multiphoton microscopy.

MATERIALS AND METHODS

HeLa cell culture

HeLa cells were cultured in Dulbecco's modified Eagle's medium (Sigma, St. Louis, MO) supplemented with antibiotics and 10% fetal bovine serum (Gibco, Billings, MT) at 37°C and 5% CO_2. For DNA damage experiments,

cells were seeded on glass-bottom culture dishes (MatTek, Ashland, MA) at a density of 3×10^5 cells/dish ~18 h before the experiment. Immediately before irradiation, the growth medium was removed and cells were washed and immersed in phosphate-buffered saline (PBS).

Drosophila strains and procedures

Three *D. melanogaster* lines were used. The transgenic line that expresses the histone 2B-monomeric red fluorescent protein (mRFP) fusion protein under the control of a *Gal4* upstream activation sequence was described in Zobeck et al. (23); in that study, the protein was expressed in salivary gland cells by generating a homozygous cross with the c147 *Gal4* driver line. The endogenous eGFP-tagged TopI fusion line was obtained from the FlyTrap stocks (line CC01414) (24). The w^{1118} line and the c147 *Gal4* line were obtained from the Bloomington *Drosophila* Stock Center (Bloomington, IN). Larva were raised at room temperature, collected at the third-instar stage eight to nine days after eggs were laid, and dissected in Grace's insect medium (Gibco). Salivary glands were transferred to MatTek glass-bottomed culture dish in PBS for irradiation.

UV irradiation setup

UV DNA damage was generated with a Spectroline Crosslinker (Westbury, NY) containing low-pressure mercury vapor lamps ($\lambda_{max} = 254$ nm). HeLa cells were irradiated in PBS to receive a dosage of ~1.6 kJ/m^2. *Drosophila* salivary glands were irradiated in PBS to receive a dosage of ~6.6 kJ/m^2.

Laser apparatus for producing DNA photolesions

To investigate multiphoton-absorption-induced photolesion formation, HeLa cell monolayers or *Drosophila* salivary glands were irradiated by focused near-IR or visible ultrashort pulses using the apparatus diagrammed in Fig. 1 *B*. Our setup used tunable near-IR femtosecond pulses produced at 80 MHz by a Chameleon Ultra II Ti:sapphire oscillator (Coherent, Santa Clara, CA). An electro-optic modulator and polarizer placed directly after the laser controlled the intensity used for each experiment. The near-IR pulse duration was 200 fs at 750 nm, as determined by a background-free autocorrelator placed just after the modulator/polarizer. As indicated, most experiments used pulses at the second harmonic of the Ti:sapphire output wavelength, which were generated by focusing the beam into a 2-mm-pathlength β-barium borate (BBO) crystal cut for type I phase matching. The residual near-IR light was rejected with a contrast ratio of at least 100:1 by reflecting the visible beam off of two dichroic mirrors before introducing it into a home-built laser-scanning microscope. The duration of the visible pulses before entering the microscope was 210 fs at 425 nm, which was determined by background-free cross correlation with the near-IR pulses. The pulses are further broadened by lenses in the laser scanner and the objective lens; we did not measure the pulse duration after the objective, but we estimate that the 425-nm pulse duration is ~450 fs at the sample (details of this calculation are provided in the Supporting Material). For experiments that use the near-IR pulses directly, we estimate that the 750-nm pulse duration is 275 fs at the sample.

The laser-scanning setup was based on an Olympus IX81 inverted microscope with a dedicated laser port. External galvanometer-mounted mirrors and relay lenses determined the angle with which the laser beam enters a 60×, 1.20 NA water-immersion objective lens. All experiments used a 0.05-μm/μs scan rate and a pixel size of 0.1 μm, resulting in a single-pixel dwell time of 2 μs/frame. Most experiments generated damage by scanning a selected region multiple times; for each experiment, we report the total pixel dwell time, which is the product of the number of passes and 2 μs. The back aperture of the lens was slightly overfilled to maintain a tight focus. The irradiation power was measured after the objective using a calibrated power meter. For damaging DNA in salivary gland cells, the mRFP-histones were excited by the same laser at a greatly reduced power (<1 mW), and the resulting epifluorescence was detected by a GaAsP photomultiplier tube in a confocal setup. Using in-house-developed Labview-based software, a region of the chromosome was selected for multiple passes of a higher-power laser beam. For HeLa cell monolayers, phase contrast microscopy was used to locate and focus the cells before high-power laser irradiation. To perform control experiments that involved continuous-wave irradiation, a Coherent 488 nm Sapphire laser beam was introduced into the same setup by a dichroic mirror, as indicated in Fig. 1 *B*.

Multiphoton microscopy

Cells were imaged by multiphoton microscopy using the aforementioned laser-scanning microscope, except without frequency-doubling the Ti:sapphire laser output. Epifluorescence was detected by a nondescanned GaAsP photomultiplier tube.

Immunocytochemistry

After irradiation, cells or glands were fixed in methanol for 15 min at −20°C, washed thrice with a solution of PBS and 0.1% (v/v) Triton-X-100 (PBT), and then blocked in PBT with 1% (w/v) bovine serum albumin (BSA) for 1 h. Samples were incubated in mouse monoclonal anti-CPD antibody (Kamiya Biomedical, Seattle, WA) solution in PBT, 1% BSA overnight at 4°C. After washing, immunofluorescence was accomplished with Alexa Fluor 488 conjugated to goat anti-mouse IgG (Invitrogen, Carlsbad, CA) in PBT, 1% BSA for 2 h at room temperature. After washing, glands were imaged in PBT using the two-photon microscopy setup described above. Alexa Fluor 488 fluorescence was excited by two-photon absorption of 900 nm and detected by a 535/60 bandpass filter. Likewise, mRFP fluorescence was excited by two-photon absorption of 1000 nm and detected by a 630/100 bandpass filter. HeLa cells were imaged by phase-contrast microscopy and wide-field immunofluorescence (470/40 excitation filter and 525/50 emission filter), both using a 20× objective.

Quantification of fluorescence images

Fluorescence images were processed using MATLAB (The MathWorks, Natick, MA) software. For HeLa cells, damaged nuclei were distinguished from the background by creating a mask from images that had been smoothed by a lowpass Gaussian filter. The unfiltered immunofluorescence intensity within each masked nucleus was averaged and the nonspecific background staining subtracted to generate a data set. Error bars represent the standard deviation among different data sets. At least three ($n \geq 3$) different data sets are averaged for each power or wavelength. Each data set contains between 20 and 40 nuclei. Immunofluorescence in polytene cells was quantified by averaging the pixels above the nonspecific background threshold inside a damaged region. The average value of the nonspecific background was then subtracted from the immunofluorescence intensity. TopI-GFP recruitment or bleaching in polytene cells was processed in a similar way, except that masks of the irradiated and unirradiated regions of each nucleus were generated from a projection of the maximum pixel intensity for all times. The same masks were then applied to each image to determine the fluorescence intensity at each time for a given nucleus. The plotted data are the average and standard deviation of intensities from three polytene nuclei, taken from different glands.

RESULTS

Immunocyctochemistry selectively stains thymine-thymine CPDs

We determined the amount of DNA damage in cells using an immunofluorescence-based assay with a CPD-specific

antibody (25,26). To validate this method, HeLa cell monolayers were irradiated by UV light (Mercury vapor, 254 nm) at an approximate dosage of 1.6 kJ/m^2. *Drosophila* salivary glands dissected from a fly line that expresses mRFP-tagged H2B histones (23) were irradiated at an approximate UV dosage of 6.6 kJ/m^2. The cells and glands were each fixed, incubated with the anti-CPD antibody, and visualized after staining with an Alexa Fluor 488-labeled secondary antibody (Fig. 1 *C*). In comparison with phase-contrast images, the immunofluorescence of the HeLa cells is uniformly distributed within cell nuclei. In the salivary glands, the brightest regions of immunofluorescence colocalize with the mRFP fluorescent protein, which marks the polytene chromosomes in cell nuclei. In both organisms, immunofluorescence in the UV-exposed samples was >10 times brighter than the control. The immunofluorescence intensity increases linearly with UV dosage (Fig. S1 in the Supporting Material).

Use of high-intensity IR pulses results in physical damage

Previous reports demonstrate that UV-like lesions, including thymine CPDs, result from multiphoton absorption of near-IR femtosecond pulses (12,17,18). However, we found that irradiation of unstained HeLa cells or polytene cells with near-IR pulses at intensities necessary to produce CPDs also disrupted their physical structure. Fig. 2 presents HeLa cells and a salivary gland that had been irradiated with focused 750-nm femtosecond pulses at an average power of 80 mW, which is approximately the minimal power that allowed for the detectable creation of CPDs with near-IR pulses (Fig. S2). Similar irradiation conditions were required to produce DNA damage in previous studies (12). Unfortunately, irradiated HeLa cells are either destroyed or exhibit pronounced morphological changes in the phase-contrast images. Likewise, irradiation of salivary glands results in the appearance of localized structures that may be due to the formation of cavitation bubbles. These results are not particularly surprising, since several groups have performed laser-based cellular nanosurgery and ablation using nearly identical irradiation conditions (19–22). Previous studies that generated DNA photolesions with near-IR pulses have limited irradiation to subnuclear regions in cultured cells, which either prevented or masked this type of unwanted cellular damage. However, it becomes difficult to avoid when studying optically thick tissue samples, such as salivary glands containing polytene nuclei. The introduction of unwanted cellular damage is not desirable for imaging DNA repair dynamics in live cells, so there is a clear need to develop an alternative method to create localized lesions that does not significantly disrupt other cellular processes.

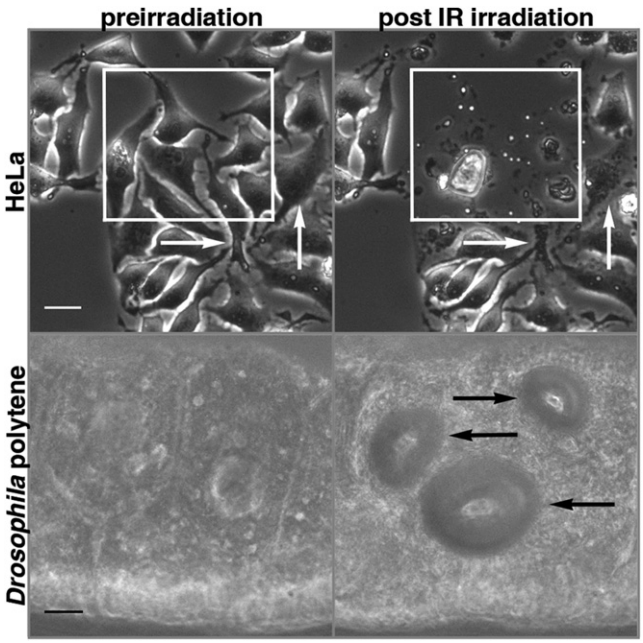

FIGURE 2 Irradiation with high-intensity IR pulses at 750 nm and 80 mW, which is approximately the minimal power required to induce thymine CPDs with near-IR light, results in unintended damage of cells. As shown by phase-contrast microscopy, the HeLa cells in the area irradiated by the IR beam (indicated by a white box) are obliterated, leaving behind only portions of the cell that can be stained for CPDs. Portions of cells that had been partially irradiated (*white arrows*) survive but also show damage. Likewise, *Drosophila* salivary gland cells exhibit pronounced morphological changes (*black arrows*) as a result of irradiation with the IR pulses. Scale bars, 30 μm.

Femtosecond visible pulses induce localized thymine CPD formation in HeLa cells

Our previous in vitro study (16) indicated that the two-photon absorption cross section of DNA is largest at 425 nm, so we started at this wavelength to investigate DIMED-Vis in vivo. Visible femtosecond pulses generated by frequency-doubling the near-IR output of a Ti:sapphire oscillator were focused into a monolayer of unstained HeLa cells by a 60×, 1.2 NA objective lens. The beam (80 MHz repetition rate, 14 mW average power after the objective) was raster-scanned over a square region of cells, resulting in a total pixel (~0.1 μm^2) dwell time of 20 μs. Cells were then fixed, stained for CPD production, and imaged using widefield fluorescence microscopy (Fig. 3 *A*). The immunofluorescence clearly demonstrates DNA damage in the nuclei of cells within the square region that had been irradiated by visible femtosecond pulses. Cells outside of the irradiated region exhibit only background fluorescence equivalent to the amount of nonspecific staining of unirradiated samples from the UV control. It is notable that cells at the boundary of the irradiated region show a sharp intranuclear boundary between the damaged and undamaged regions. It is important to note that the phase-contrast image shows no physical malformations of the irradiated HeLa

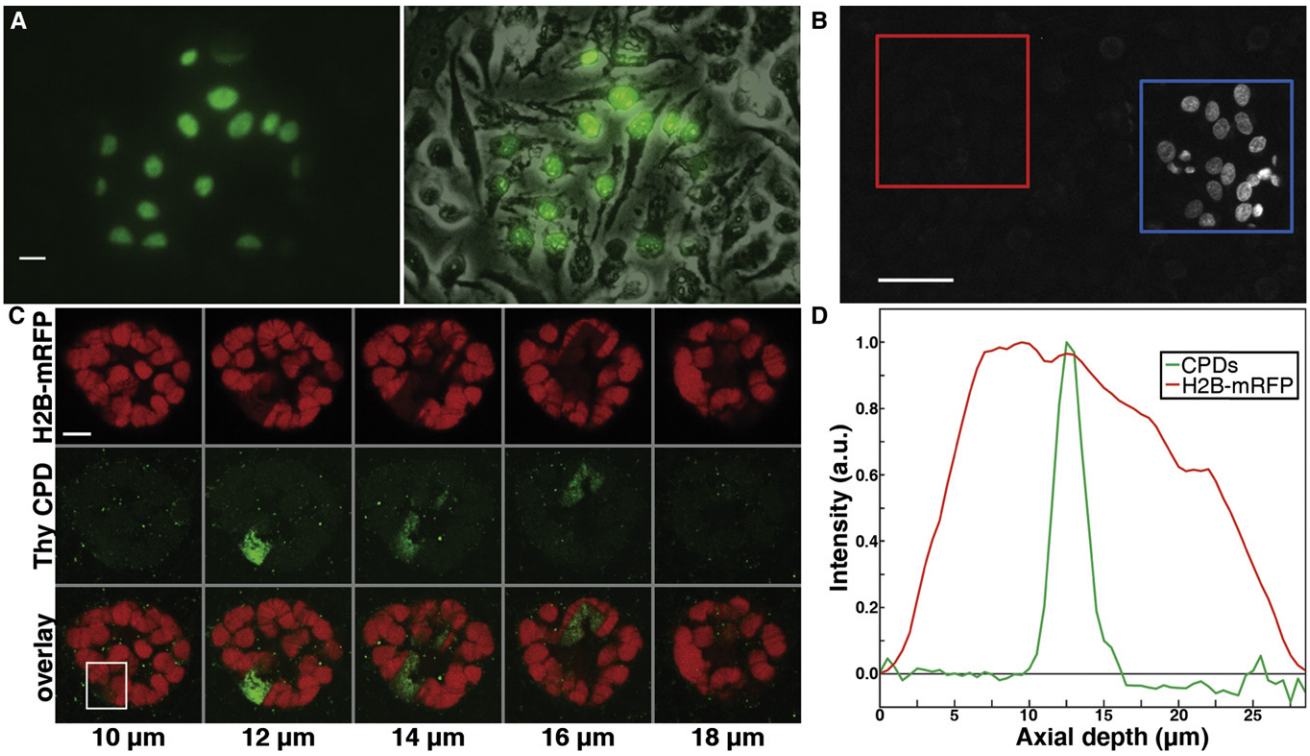

FIGURE 3 Production of CPDs using 425-nm femtosecond pulses. (*A*) (*Left*) HeLa cells were irradiated by femtosecond pulses in a square region that included intra-and extranuclear regions, then stained for CPDs and imaged with wide-field epifluorescence. Only cells inside the irradiation region show immunofluorescence, even though there are cells outside of this region. Furthermore, the immunofluorescence is confined to nuclear regions only, although the entire cell was irradiated. (*Right*) The overlay on the phase-contrast image demonstrates that CPDs are laterally confined, even in nuclei of cells that were only partially irradiated. Scale bar, 20 μm. (*B*) The generation of thymine CPDs due to visible laser light is due to a nonlinear process; therefore, the required photon flux (GW/cm^2) can only be achieved with a pulsed laser. HeLa cells were irradiated with light at 488 nm and 13 mW average intensity from a 150-fs pulsed laser (*blue box*) and a CW laser source (*red box*), each focused by the same 60× 1.2 NA objective lens. Only the pulsed laser source created thymine CPDs, further indicating that the production of thymine CPDs with visible light is a nonlinear process. The outline boxes are slightly larger than the irradiated region to prevent obscuring of the epifluorescence. Scale bar, 16 μm. (*C*) Selected slices from a *z*-series of a *Drosophila* polytene nucleus that had been irradiated by femtosecond pulses in a rectangular region before staining. The CPDs are axially confined to a region much smaller than the depth of the nucleus. The orientation of the gland when it was imaged after the CPD staining procedure is different from that when it was damaged; therefore, the damage and bleach shifts across the gland through the *z*-series. The contrast of images was uniformly enhanced to assist in viewing. Scale bar, 5 μm. (*D*) Quantification of the CPD immunofluorescence in the white box in *C*, and the mRFP fluorescence for the entire cell. The intensity of the mRFP-labeled H2B histone (*red line*) and the immunofluorescence labeling of CPDs (*green line*) are plotted as a function of the axial depth of the sample. The nucleus is approximately spherical, 20 μm (full width at half-maximum) in diameter. The region of the production of photolesions is confined to an ~2.5-μm-thick (full width at half-maximum) region of the chromosome.

cells, in contrast to irradiation with near-IR pulses. To demonstrate that DNA damage is caused by multiphoton absorption and exclude the possible involvement of endogenous sensitizers, we compared irradiation of HeLa cells with a beam of ultrashort visible pulses to irradiation with a continuous-wave (CW) beam at the same wavelength and power (Fig. 3 *B*). The thymine CPDs were only produced when using pulsed sources of light, demonstrating that the high peak intensities of femtosecond pulses are necessary to generate CPDs.

Thymine CPDs are axially localized

We also investigated the generation of CPDs via DIMED-Vis in polytene cells. To locate cell nuclei, salivary glands that express histone H2B-mRFP fusion proteins were imaged using confocal microscopy, excited by the 425-nm beam of femtoseond pulses at a reduced power (<1 mW). Selected regions of cells were then irradiated by the same beam at a higher power to generate DNA damage (10 mW average power and a 10-μs total pixel dwell time). The glands were subsequently fixed and stained for CPD production. The immunofluorescence and mRFP were imaged using standard two-photon microscopy (Fig. 3 *C*). The applied laser light bleaches the mRFP, marking the location of high-power laser irradiation. The immunofluorescence colocalizes with the mRFP bleach, establishing that CPDs had been created in the region irradiated by the high-power beam of 425-nm femtosecond pulses. Only a thin axial region (2.5 μm FWHM) contained the CPDs (Fig. 3 *D*), implying that the damage was due to multiphoton absorption. The intensity used to ensure a strong staining probably

saturated the multiphoton absorption, resulting in a thicker axial section than would be expected based on the theoretical diffraction-limited point spread function of the objective lens. Note that the orientation of the gland when the immunofluorescence was imaged differed slightly from its orientation when the damage was generated, resulting in CPDs that are localized on opposite sides of the nucleus in subsequent optical sections. Chromosomes outside of the region irradiated with the high power beam exhibit the same amount of immunofluorescence and mRFP fluorescence as those in unirradiated glands. This observation confirms that the lower power used for confocal imaging does not generate damage, as would be expected for a nonlinear intensity dependence. Finally, since it is possible that the presence of a fluorescent histone protein fusion could sensitize DNA to photodamage, we confirmed that the same numbers of CPDs are created in the nuclei of salivary glands that do not express a fluorescent marker (Fig. S3).

Thymine CPDs are produced with 400–525-nm femtosecond pulses

To determine the ideal wavelength for CPD production, HeLa cells were irradiated with various wavelengths of visible pulses, ranging from 400 to 525 nm at 25-nm intervals, and subsequently assayed for the number of CPDs produced. The same power and pixel dwell time were used at each wavelength within a particular data set. CPDs were created at each wavelength tested, though there is a clear maximum at 400 nm and a general trend of decreasing efficiency with wavelength (Fig. 4 *A*). The large multiphoton absorption cross section difference between 400 and 425 nm is somewhat surprising, since the UV absorption spectrum is quite broad, but the similar cross sections from 425 to 475 nm agree with our previous in vitro findings (16). It should be noted that the lower efficiency at longer wavelengths can easily be overcome by using higher powers. The ability to create CPDs over a broad range of wavelengths allows for the tailoring of a damage method according to the fluorophore being used in a given study: the damaging wavelength can be chosen to minimize or maximize fluorophore bleaching depending on the experiment.

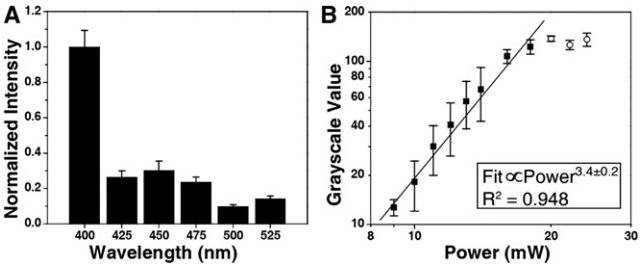

FIGURE 4 Characterization of the photophysical parameters that lead to the production of CPDs. (*A*) The production of CPDs was quantified in HeLa cells using various irradiation wavelengths from 400 to 525 nm at 25-nm intervals. Error bars represent the standard deviation among the average intensities of cells in three different irradiation regions. (*B*) HeLa cells were irradiated at 425 nm from 6 to 24 mW and data are plotted on a log scale. Data points at 6, 7, and 8 mW were below the threshold of detection and are not plotted. Points included in the regression are represented by solid squares and those excluded due to saturation as open circles. The fit scales with the irradiation power raised to the 3.4 ± 0.2 power with a coefficient of determination of 0.948. Error bars are standard deviations among the average intensities of cells in three different irradiation regions ($n = 3$).

Power dependence of thymine CPD production

We examined the intensity dependence of CPD production by irradiating HeLa cells with 425-nm femtosecond pulses at various powers, ranging from 6 to 24 mW (Fig. 4 *B*). Based on the strong 200- to 300-nm UV absorption of DNA that leads to CPD production, as well as on our previous in vitro results, we expected that the amount of damage would scale with the square of the applied laser power, indicating a photochemical mechanism involving two-photon absorption. We were somewhat surprised to find that the data are fit best by a supercubic (3.4 ± 0.2) function of incident power, implicating higher-order nonlinearities. The 425-nm light was tested because it allowed for a relatively large range of powers to be tested, but similar results were obtained at 400 nm (3.0 ± 0.5) and 500 nm (3.5 ± 0.2).

Recruitment of topoisomerase I to DNA photolesions in polytene cells

To assess the utility of DIMED-Vis for investigating the dynamics of protein recruitment to spatially localized CPDs, we studied the localization of TopI in polytene cells after irradiation with visible femtosecond pulses. TopI is an enzyme that changes the topology of DNA by introducing a transient break in one strand of its backbone, through which the other strand can pass. TopI activity has previously been implicated in transcription, replication, and repair (27); it is essential for the viability of multicellular organisms, including *Drosophila* (28). Using multiphoton microscopy, we imaged the localization of TopI-GFP fusion proteins in polytene cells from a GFP protein-trap fly line (24). Before DNA damage induction, TopI-GFP is localized within the nucleus and exhibits well-defined banding along polytene chromosomes, as well as diffuse localization between bands and within the nucleoplasm (23). Irradiation of approximately one-quarter of the nucleus in a single axial plane with intense 425-nm femtosecond pulses (10 mW, 10 μs total pixel dwell time) completely bleaches the GFP fluorescence within the selected region. Fluorescent TopI-GFP subsequently diffuses into the selected region, starting from its intranuclear boundaries and reaching an equilibrium fluorescence distribution within 3–4 min (Fig. 5 *A*). Fluorescence of TopI-GFP outside the selected region decreases on the same timescale to a final intensity

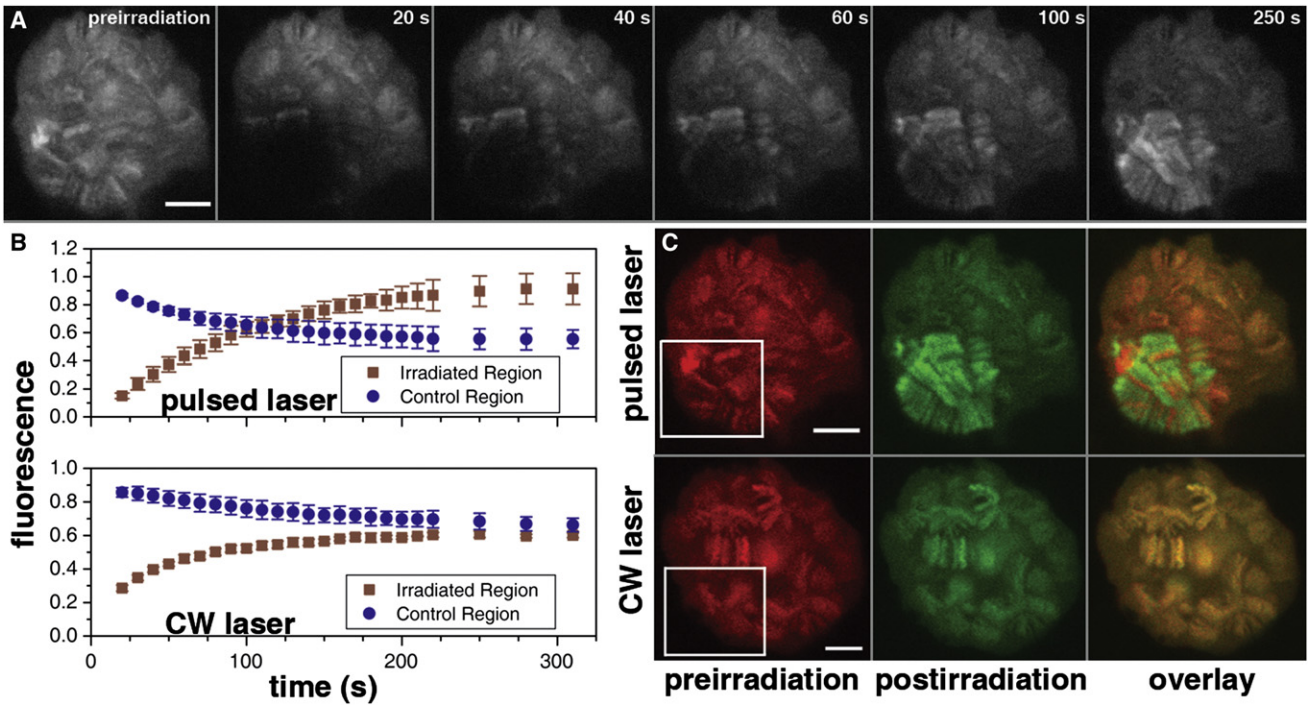

FIGURE 5 Localization of TopI to DNA photolesions. Scale bars, 5 μm. The contrast of images was uniformly enhanced to assist in viewing. (*A*) DNA in a *Drosophila* polytene cell that expresses a TopI–GFP fusion protein was damaged using DIMED-Vis by irradiating the lower left quadrant of a single nuclear plane with 425 nm femtosecond pulses. The irradiation also bleaches the GFP fluorescence in the damaged region. Multiphoton microscopy images recorded as a function of time after irradiation reveal that fluorescent TopI-GFP preferentially accumulates in the damaged region, beginning with the intranuclear edges and subsequently populating the entire region. (*B*) (*Upper*) The integrated fluorescence intensity in the damaged region (*squares*) recovers to a value close to its initial intensity, whereas the integrated fluorescence in the unirradiated region (*circles*) decreases below this value. (*Lower*) By contrast, under similar conditions, the fluorescence in nuclei irradiated by a 488-nm CW laser, which bleaches GFP but does not generate DNA damage, recovers to the same value in the irradiated and unirradiated regions. Plots are normalized to the preirradiation intensity. Error bars represent the standard deviation among three different cell nuclei ($n = 3$). (*C*) (*Upper*) For the cell damaged in *A*, the preirradiation TopI-GFP fluorescence distribution (*red*) within the irradiated region (*white box*) antilocalizes with the TopI-GFP fluorescence distribution in the postirradiation (after 250 s) fluorescence image (*green*). (*Lower*) In contrast, a cell irradiated by the CW laser exhibits the same TopI-GFP fluorescence distribution in the pre- and postirradiation images.

that is significantly less than the final intensity within the selected region (Fig. 5 *B*). This intensity difference likely arises from the preferential accumulation of TopI-GFP at DNA damaged by multiphoton absorption of visible pulses, in agreement with previous studies that observed TopI recruitment to the site of DNA photolesions (29,30). This interpretation is also supported by a post-damage *z*-series that shows that TopI-GFP is axially localized to the irradiated region, similar to the axial profile of CPDs (Fig. S4). To test our interpretation that TopI-GFP preferentially localizes to damaged DNA, we irradiated nuclei with a 488-nm CW laser, which bleaches GFP but does not damage DNA. As expected, the bleached and unbleached regions recover to the same final intensity (Fig. 5 *B*). It is interesting to note that the TopI-GFP banding pattern after DNA damage with visible femtosecond pulses largely antilocalizes with the banding pattern before damage. In contrast, cells irradiated by the CW laser exhibit the same banding pattern before and after bleaching (Fig. 5 *C*). These observations are consistent with a model in which TopI associates with DNA transiently in the absence of damage, but localizes to damaged sites more stably, as discussed below.

DISCUSSION

For the study of DNA repair-protein dynamics, it is desirable to produce spatially localized damage sites to observe the mechanism by which repair proteins locate damage sites. The direct multiphoton absorption of DNA creates spatially confined photolesions ideal for the observation of the recruitment of repair proteins to the damage site. In this report, we have damaged large regions of the chromosome for the purpose of quantifying and observing immunofluorescence, but it would be straightforward to create damage only in a diffraction-limited spot, ~200 $\times$ 200 $\times$ 500 nm.

Previous attempts at producing DNA damage via multiphoton absorption have focused on near-IR pulses, which require millisecond pixel dwell times (18), very intense pulses, or chemical sensitizers (12). Our current setup configuration was optimized for microsecond (rather than

millisecond) dwell times, which is typical for multiphoton and confocal microscopes. However, we did determine that the conditions required to create DNA damage using high intensity IR pulses also resulted in other unwanted damage to the cells when large scan regions were used (Fig. 2). We note that the large regions irradiated in this study created more severe damage than if a smaller region were chosen, but even localized, intranuclear near-IR irradiation that preserves the cell's macrostructure likely causes unwanted disturbances. Our results are consistent with earlier reports that similar irradiation conditions can dissect chromosomes (22), induce strand breaks (12,18), and invoke cell death (21). Thus, DIMED with near-IR pulses is undesirable for the study of protein dynamics in thick tissues where multiple cells are damaged. Furthermore, the chemical sensitization of DNA, although it allows for the use of nonlethal irradiation intensities, can adversely affect the DNA repair pathway under study and preferentially results in non-UV-type lesions. By using 25- to 44-ms pixel dwell times, as presented in the reports by Meldrum et al. (17) and Trautlein et al. (18), the powers needed to generate DNA photolesions may be below the threshold for unintended cellular damage. However, even scanning a small area (~10 $\times$ 10 pixels) requires several seconds, thus reducing the time resolution to measure the protein response, and such long pixel dwell times can be difficult to implement on some laser-scanning microscopes.

The method characterized in this article, DIMED-Vis, allows for the production of axially localized CPD type photolesions in thick tissues without physical damage to the cell, providing a useful alternative to previously reported methods of creating damage. In addition, it is relatively easy to implement by modifying an existing two-photon microscopy setup with the addition of a frequency-doubling BBO crystal. We have shown that DIMED-Vis works on two very different cell types. It is especially powerful when paired with the polytene nucleus of *Drosophila* larva salivary gland, since the large chromosomes of the polytene nucleus allow regions of DNA to be distinguished from nucleoplasm. However, the large nuclei present the need for axial confinement, which our method addresses. The successful use of DIMED on cells containing polytene chromosomes and diffuse chromatin and with or without transgenic fluorescent markers indicates its flexibility. The observed wavelength dependence was somewhat unexpected; in particular, it is unclear why CPDs are produced more efficiently with 400-nm pulses than with the other observed wavelengths, since such sharp transitions are not observed in the UV absorption spectrum of DNA. At the measured wavelengths of 400, 425, and 500 nm, the production of CPDs all scaled with an approximate cubic power dependence. Therefore, it can be reasonably concluded that the same transition is being excited at each wavelength. However, it is important to note that CPDs can be efficiently produced at all wavelengths tested, thereby granting the flexibility to choose a damaging wavelength that is most appropriate considering other parts of the experiment, such as minimizing fluorophore photobleaching.

We expect DIMED to produce UV-type lesions which is why we tested for thymine-thymine CPDs, the primary UV photoproduct. Several observations point toward the direct multiphoton absorbance of DNA as the source of photolesion formation, indicating that the photoreactions should be UV-like. The applied visible pulses are off-resonant for DNA linear absorption; the linear absorption of the nitrogen bases is strongest between 200 and 300 nm and is completely transparent in the range 400–525 nm. Therefore, the damage is due either to the multiphoton absorption of DNA or through the sensitization of damage by other fluorophores (e.g., mRFP). However, as shown in HeLa cells and polytene cells devoid of fluorophores, we can induce CPDs in cells without fluorescent proteins. This evidence excludes mRFP as a possible sensitizing agent. Furthermore, when using a CW laser at the same wavelength and time-averaged power as a pulsed laser, the thymine CPDs are not produced. The production of the photolesions using blue light, therefore, requires the high peak intensities provided by an ultrashort-pulsed laser, indicative of nonlinear excitation of DNA and excluding linearly absorbing sensitizing agents (Fig. 3 *B*). Finally, the power series is nonlinear, indicating a multiphoton process (Fig. 4 *B*). Although the cubic power dependence was unexpected, others (18) have shown higher-order nonlinearities in the formation of thymine CPD using IR pulses. Therefore, the observed DNA damage is likely due to multiphoton excitation of DNA. We cannot be certain the damage is not mediated by multiphoton absorption of a secondary species, such as histones, but we believe this interaction is unlikely, because such a mechanism would preferentially create strand breaks with few, if any, CPD photoproducts. Other types of UV photolesions are also likely produced by DIMED-Vis, such as 6-4 photoproducts. We do not expect to form a large quantity of double strand breaks, as these are not typically produced by UV exposure; however, near-IR ultrafast irradiation has resulted in the production of double strand breaks. In the future, we plan to measure the distribution of lesions to determine how DIMED-Vis compares to other published methods of DNA damage induction.

We have demonstrated one application of DIMED-Vis by measuring the time-resolved localization of TopI-GFP to a region of damaged DNA in polytene cells. After inducing DNA photodamage, TopI-GFP accumulates within the irradiated region of the nucleus and is depleted in the unirradiated region (Fig. 5), indicating that TopI is recruited to damaged DNA (CPDs and other potential types of damage). This observation strengthens earlier suggestions (27) that TopI is involved in DNA damage repair. However, the application of DIMED-Vis in polytene cells offers much more information about the spatiotemporal dynamics of TopI

than is available using other methods. After localized damage, the fluorescent protein is confined within a 2-μm axial plane (Fig. S4) and exhibits antilocalized banding compared to the preirradiated image. We presume that the TopI-GFP that had been in the irradiated region before damage associates stably with the newly damaged DNA but is no longer visible because the GFP is bleached. The TopI-GFP that had been in the unirradiated region thus fills in chromosomal regions that contained a lower density of TopI-GFP before damage, resulting in the observed antilocalization. In contrast, when TopI-GFP is only bleached without creating photolesions by using a 488-nm CW laser, antilocalization is not observed, since the equilibrium distribution of DNA-associated TopI-GFP is constantly exchanging. We also observe that the TopI-GFP initially exhibits a preferential localization to chromosomes near the boundary between the damaged and undamaged regions after damage, leaving the region farther from this boundary depleted for more than a minute. This behavior is not observed in nuclei bleached by a CW laser, which recover fluorescence more uniformly (Fig. S5), and is another consequence of the accumulation of TopI-GFP at damaged DNA. Finally, we note that optical resolution limits prevent us from unambiguously proving that TopI is recruited to damaged DNA on a molecular lengthscale. For example, it is also possible that DIMED-Vis changes the nuclear matrix in a way that causes TopI to be immobilized on chromosomes; however, we consider this unlikely, since the morphology of H2B-mRFP is unchanged by irradiation. We continue to investigate the spatiotemporal localization of TopI-GFP and will present a more detailed analysis in a future publication.

CONCLUSION

We have developed a method, DIMED-Vis, for creating localized DNA photolesions ideal for the study of DNA repair. We showed that photolesions could be created by laser irradiation between 400 and 525 nm in both HeLa cells and the polytene chromosomes of the *Drosophila*. The creation of thymine CPDs was confirmed through the use of an immunocytochemistry assay. As an example of the application of DIMED-Vis, we showed the recruitment of TopI to DNA photolesions, demonstrating the utility of this technique for resolving spatiotemporal dynamics of DNA repair.

SUPPORTING MATERIAL

Five figures, supporting text (Estimation of pulse duration at the sample), and reference (31) are available at http://www.biophysj.org/biophysj/supplemental/S0006-3495(11)01122-2.

Funding for this work was provided by the University of North Carolina at Chapel Hill.

REFERENCES

1. Gorner, H. 1994. Photochemistry of DNA and related biomolecules: Quantum yields and consequences of photoionization. *J. Photochem. Photobiol. B.* 26:117–139.
2. Wang, S. Y. 1976. Photochemistry and Photobiology of Nucleic Acids. Academic Press, New York.
3. Essers, J., W. Vermeulen, and A. B. Houtsmuller. 2006. DNA damage repair: anytime, anywhere? *Curr. Opin. Cell Biol.* 18:240–246.
4. Cremer, C., T. Cremer, …, K. Nakanishi. 1980. Detection of laser-UV microirradiation-induced DNA photolesions by immunofluorescent staining. *Hum. Genet.* 54:107–110.
5. Moné, M. J., M. Volker, …, R. van Driel. 2001. Local UV-induced DNA damage in cell nuclei results in local transcription inhibition. *EMBO Rep.* 2:1013–1017.
6. Moné, M. J., T. Bernas, …, R. van Driel. 2004. *In vivo* dynamics of chromatin-associated complex formation in mammalian nucleotide excision repair. *Proc. Natl. Acad. Sci. USA.* 101:15933–15937.
7. Katsumi, S., N. Kobayashi, …, T. Mori. 2001. In situ visualization of ultraviolet-light-induced DNA damage repair in locally irradiated human fibroblasts. *J. Invest. Dermatol.* 117:1156–1161.
8. Imoto, K., N. Kobayashi, …, T. Mori. 2002. The total amount of DNA damage determines ultraviolet-radiation-induced cytotoxicity after uniformor localized irradiation of human cells. *J. Invest. Dermatol.* 119:1177–1182.
9. Limoli, C. L., and J. F. Ward. 1993. A new method for introducing double-strand breaks into cellular DNA. *Radiat. Res.* 134:160–169.
10. Lukas, C., J. Falck, …, J. Lukas. 2003. Distinct spatiotemporal dynamics of mammalian checkpoint regulators induced by DNA damage. *Nat. Cell Biol.* 5:255–260.
11. Kruhlak, M. J., A. Celeste, …, A. Nussenzweig. 2006. Changes in chromatin structure and mobility in living cells at sites of DNA double-strand breaks. *J. Cell Biol.* 172:823–834.
12. Dinant, C., M. de Jager, …, W. Vermeulen. 2007. Activation of multiple DNA repair pathways by sub-nuclear damage induction methods. *J. Cell Sci.* 120:2731–2740.
13. Lakowicz, J. R. 1997. Topics in Fluorescence Spectroscopy, Vol. 5: Nonlinear and two-photon-induced fluorescence. Kluwer Academic, New York.
14. Denk, W., J. H. Strickler, and W. W. Webb. 1990. Two-photon laser scanning fluorescence microscopy. *Science.* 248:73–76.
15. Zipfel, W. R., R. M. Williams, and W. W. Webb. 2003. Nonlinear magic: multiphoton microscopy in the biosciences. *Nat. Biotechnol.* 21:1369–1377.
16. Tycon, M. A., A. Chakraborty, and C. J. Fecko. 2011. Generation of DNA photolesions by two-photon absorption of a frequency-doubled Ti:Sapphire laser. *J. Photochem. Photobiol. B.* 102:161–168.
17. Meldrum, R. A., S. W. Botchway, …, G. J. Hirst. 2003. Nanoscale spatial induction of ultraviolet photoproducts in cellular DNA by three-photon near-infrared absorption. *EMBO Rep.* 4:1144–1149.
18. Träutlein, D., M. Deibler, …, E. Ferrando-May. 2010. Specific local induction of DNA strand breaks by infrared multi-photon absorption. *Nucleic Acids Res.* 38:e14.
19. Kuetemeyer, K., R. Rezgui, …, A. Heisterkamp. 2010. Influence of laser parameters and staining on femtosecond laser-based intracellular nanosurgery. *Biomed. Opt. Express.* 1:587–597.
20. Supatto, W., D. Débarre, …, E. Beaurepaire. 2005. In vivo modulation of morphogenetic movements in *Drosophila* embryos with femtosecond laser pulses. *Proc. Natl. Acad. Sci. USA.* 102:1047–1052.
21. Tirlapur, U. K., K. König, …, K. J. Halbhuber. 2001. Femtosecond near-infrared laser pulses elicit generation of reactive oxygen species in mammalian cells leading to apoptosis-like death. *Exp. Cell Res.* 263:88–97.

22. König, K., I. Riemann, and W. Fritzsche. 2001. Nanodissection of human chromosomes with near-infrared femtosecond laser pulses. *Opt. Lett.* 26:819–821.

23. Zobeck, K. L., M. S. Buckley, …, J. T. Lis. 2010. Recruitment timing and dynamics of transcription factors at the Hsp^{70} loci in living cells. *Mol. Cell.* 40:965–975.

24. Buszczak, M., S. Paterno, …, A. C. Spradling. 2007. The carnegie protein trap library: a versatile tool for *Drosophila* developmental studies. *Genetics.* 175:1505–1531.

25. Rubbi, C. P., and J. Milner. 2003. p53 is a chromatin accessibility factor for nucleotide excision repair of DNA damage. *EMBO J.* 22:975–986.

26. Katiyar, S. K., M. S. Matsui, and H. Mukhtar. 2000. Kinetics of UV light-induced cyclobutane pyrimidine dimers in human skin in vivo: an immunohistochemical analysis of both epidermis and dermis. *Photochem. Photobiol.* 72:788–793.

27. Leppard, J. B., and J. J. Champoux. 2005. Human DNA topoisomerase I: relaxation, roles, and damage control. *Chromosoma.* 114:75–85.

28. Lee, M. P., S. D. Brown, …, T. S. Hsieh. 1993. DNA topoisomerase I is essential in *Drosophila melanogaster*. *Proc. Natl. Acad. Sci. USA.* 90:6656–6660.

29. Mao, Y., and M. T. Muller. 2003. Down modulation of topoisomerase I affects DNA repair efficiency. *DNA Repair (Amst.).* 2:1115–1126.

30. Mielke, C., F. M. Kalfalah, …, F. Boege. 2007. Rapid and prolonged stalling of human DNA topoisomerase I in UVA-irradiated genomic areas. *DNA Repair (Amst.).* 6:1757–1763.

31. Guild, J. B., C. Xu, and W. W. Webb. 1997. Measurement of group delay dispersion of high numerical aperture objective lenses using two-photon excited fluorescence. *Appl. Opt.* 36:397–401.